SOLID NITROGEN HARDNESS MEASUREMENTS AT TRITON SURFACE CONDITIONS. M. R. Maughan[1], Z. Hacker[1], J. W. Leachman[2], J. W. Hartwig[3], [1]University of Idaho, Moscow, ID, [2]Washington State University, Pullman, WA, [3]NASA Glenn Research Center, Cleveland, OH, maughan@uidaho.edu

Introduction: The largest moon around Neptune, Triton, is a unique celestial body that has a rarified atmosphere [1], active geysers as high as 8 km that leave plumes suspended in the atmosphere that can drift down wind for over 100 km [2], and could potentially have tholins [3,4]. Limited fly-by observational data [5] of this captured Kuiper Belt Object shows evidence that nitrogen is the dominant constituent, potentially also existing on other outer Solar System bodies of interest such as Pluto. Many fundamental questions remain such as:

(1) What processes cause Triton's geysers?
(2) Are the plumes on Triton caused by the solid-state greenhouse effect?
(3) What processes drive the cycle of volatiles between Triton's surface and atmosphere?

Numerical simulations required to address these questions as well as the development of future mission science packages and vehicles [6] require accurate, reliable thermodynamic and mechanical property data of solid and gaseous nitrogen at relevant surface and atmospheric conditions.

The surface of Triton is estimated to be at 1.6 Pa [1] and have a temperature range between 30-40 K [2,7]. This temperature range straddles the nitrogen α to β phase transformation temperature, 35.61 K [8]. A recent thorough and exhaustive review of the literature [9] revealed that mechanical property data on solid nitrogen (SN_2) is extremely sparse, with only three known physical strength measurements reported in the literature [10–12]. What follows is the description of experimental hardware and test results of the most recent set of SN_2 hardness measurements conducted between 30 – 40K.

Methods: The instrumented hardness tester interfaces with a custom-built cryostat. The 0.48 x 0.57 x 0.28 m stainless steel vacuum chamber is evacuated by a Leybold DB8 rotary vain vacuum pump in line with an Agilent Tv 81m turbomolecular pump. Cooling is provided by a Cryomech PT405 pulse-tube cryocooler with a copper thermal radiation shield surrounding the test cell and cooled through the first stage of the cryocooler.

The instrumented indentation system uses a commercially available 45 kg screw-driven load frame. A custom microcontroller system provides vertical motion control via a stepper motor and force measurement via an S-beam load-cell with appropriate signal amplification. The load cell is connected between the cross-head of the load frame and the vertical indentation shaft outside the cryostat. The shaft then passes through a double o-ring seal, into the upper part of the cylindrical specimen chamber. The upper specimen chamber bolts to a bus-bar where heat is transferred away to the cryopump. The lower specimen chamber comprises a cylindrical copper cup, also bolted by a flange to the bus-bar. Bolted connections were sealed via crushed indium gaskets. Inside the lower specimen chamber, a copper cross-bar is mounted to the end of the indenter shaft and the titanium indenter probe is threaded into the lower surface of the cross-bar. This permitted offsetting the indenter from centerline allowing for multiple indents per sample without the need to heat to liquid then solidify between tests.

Temperatures of the sample were measured and controlled by a Lakeshore 336, germanium resistance temperature detector (RTD) and heater attached to the outside of the lower specimen chamber. Accuracy of the sensor was ± 0.2 K, the majority of samples were taken within 0.2 K of their target temperature leaving control uncertainty of approximately 0.3 K. The indenter temperature was measured at the copper cross-bar via a platinum RTD with an uncertainty of 0.25 K. Thermal equilibrium was achieved by bringing the indenter into contact with the specimen. After cooling the indenter in the sample, the crossbar temperature was measured at approximately 1.5 K above the sample temperature. Considering the temperature probe location, low thermal mass of indenter, and thermal dead-end nature of the specimen container, it can be presumed that any temperature difference between sample and indenter was much less than 1.5K during data collection. Once the probe had cooled (approximately 20 minutes), the indenter head was lifted and rotated to the desired position for testing. The apparatus is shown schematically in Fig. 1.

A flat punch indenter geometry was used because this made surface detection via analysis of the force vs. displacement data straightforward. Another benefit of the flat punch geometry is that a description of the projected area versus contact depth (area function) is not required for pressure analysis. Two indenter diameters (2.25 and 2.77 mm) were used throughout the temperature range to stay within the load capacity of the load frame and provide maximum resolution of the corrected force result.

Due to drag from the O-ring seals, the indenter was calibrated at temperature with no sample. The calibration force data were subtracted in post-

processing from the data collected from the specimens. This process was verified by substituting springs of known spring constant for the sample and showed acceptable results.

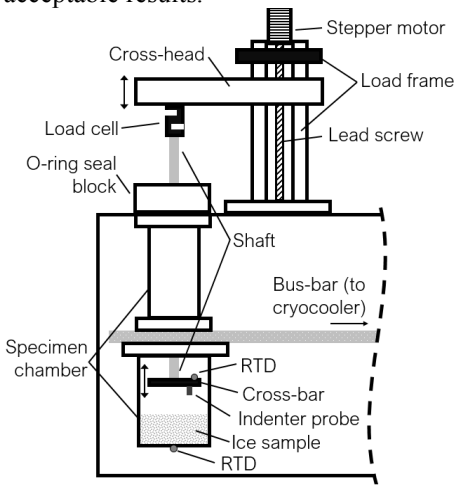

Figure 1: Schematic representation of insutrumented indentation tester and cryostat. The lower specimen chamber is shown in cross-section.

Results: The behavior of the SN_2 changed considerably over the 10K range studied. Fig. 2 shows the pressure developed at the indenter surface versus displacement for several temperatures. Zero diplacment corresponds to initial contact with the sample surface. Note that indentation testing in traditional engineering materials would never be conducted to such large displacements relative to indenter diameter, but can be included here for increased understanding of the material behavior. The curves show increasing pressure with increasing indenter penetration. This may indicate some degree of strain hardening in the material under confined compression conditions. At lower temperatures, a distinct reduction in pressure can be seen around 3.5 mm displacement into the sample.

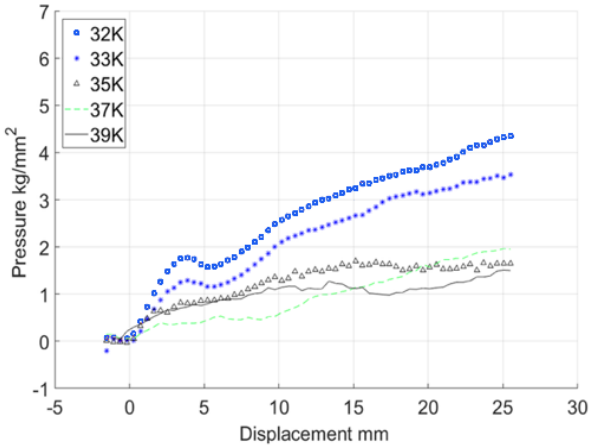

Figure 2: Pressure versus indenter penetration depth curves for various temperatures.

Due to the pressure reduction, hardness values are calculated at the peak load before the drop. These ranged from 0.5 kg/mm^2 to 2 kg/mm^2. Trepp reported hardness between ~0.15 kg/mm^2 and ~0.6 kg/mm^2 in a similar range. Our results are somewhat harder due to several potential factors: 1) selection of peak load for hardness calculation, 2) stainless steel indenter and structure in the previous experiment, 3) voids or bubbles samples in previous experiments due to formation method.

Acknowledgements: The authors wish to acknowledge the NASA Innovative Advanced Concepts office which funded this work via grants numbered 80NSSC19K0250 and 80NSSC19K0251.

References: [1] D.P. Cruikshank, T.L. Roush, T.C. Owen, T.R. Geballe, C. de Bergh, B. Schmitt et al., *Ices on the Surface of Triton*, Science 261 (1993), pp. 742–745. [2] L.A. Soderblom, S.W. Kieffer, T.L. Becker, R.H. Brown, A.F. Cook, C.J. Hansen et al., *Triton's Geyser-Like Plumes: Discovery and Basic Characterization*, Science 250 (1990), pp. 410–415. [3] E. de Vanssay, G.D. McDonald and B.N. Khare, *Evidence from scanning electron microscopy ofexperimental influences on the morphology of Triton and-Titan tholins*, Planet. Space Sci. 47 (1999), pp. 433–440. [4] G.D. McDonald, W.R. Thompson, M. Heinrich, B.N. Khare and C. Sagan, *Chemical Investigation of Titan and Triton Tholins*, Icarus 108 (1994), pp. 137–145. [5] B.A. Smith, L.A. Soderblom, D. Banfield, c. Barnet, A.T. Basilevsky, R.F. Beebe et al., *Voyager 2 at Neptune: Imaging Science Results*, Science 246 (1989), pp. 1422. [6] G. Landis, S. Oleson, P. Abel, M. Bur, A. Colozza, B. Faller et al., Missions to Triton and Pluto using a Hopper Vehicle with In-Situ Refueling, 2019. [7] E. Quirico, S. Douté, B. Schmitt, C. de Bergh, D.P. Cruikshank, T.C. Owen et al., *Composition, Physical State, and Distribution of Ices at the Surface of Triton*, Icarus 139 (1999), pp. 159–178. [8] V.G. Manzheliĭ and Y.A. Freiman, *Physics of Cryocrystals*, American Institute of Physics, Woodbury, NY, 1997. [9] D. Sagmiller and J. Hartwig, *Survey of Cryogenic Nitrogen Thermo-Mechanical Property Data Relevant to Outer Solar System Bodies*, Earth Space Sci. accepted for publication . [10] C. Trepp, Schweiz. Arch. Angew. Wiss. Tech. B24 (1958), pp. 230. [11] A.V. Leonteva, Yu.S. Stroilov and I.N. Krupskii, in Fiz. Kondens. Sostoyan, XVI (1971). [12] Y. Yamashita, M. Kato and M. Arakawa, *Experimental study on the rheological properties of polycrystalline solid nitrogen and methane: Implications for tectonic processes on Triton*, Icarus 207 (2010), pp. 972–977.